Conference on Modelling Fluid Flow (CMFF'22)
The 18th International Conference on Fluid Flow Technologies
Budapest, Hungary, August 30 -September 2, 2022

THE INVESTIGATION OF COUNTER-ROTATING TURBOMACHINERY BROADBAND NOISE SOURCES AS A FUNCTION OF ROTATIONAL SPEED

Ádám ROMASZ[1], Kristóf TOKAJI[2], Csaba HORVÁTH[3]

[1] Department of Fluid Mechanics, Faculty of Mechanical Engineering, Budapest University of Technology and Economics. Bertalan Lajos u. 4 – 6, H-1111 Budapest, Hungary. E-mail: romasz.adi99@gmail.com
[2] Department of Fluid Mechanics, Faculty of Mechanical Engineering, Budapest University of Technology and Economics. Bertalan Lajos u. 4 – 6, H-1111 Budapest, Hungary. E-mail: tokaji.kristof@gpk.bme.hu
[3] Department of Fluid Mechanics, Faculty of Mechanical Engineering, Budapest University of Technology and Economics. Bertalan Lajos u. 4 – 6, H-1111 Budapest, Hungary. E-mail: horvath.csaba@gpk.bme.hu

ABSTRACT

Counter-rotating turbomachinery often appear in modern aerospace applications. Along with their numerous advantageous properties they are also known to produce high amounts of noise. The emitted noise consists of tonal and broadband noise components, which can be studied utilizing beamforming technology. In order to analyse them more efficiently and reach a better understanding of the noise generation mechanisms, these noise components must be separated. The Double Filtering Method allows one to separate these two noise source categories, making it possible to examine broadband noise components without any interference from tonal noise components. In this paper a series of studies are carried out on various parameters that influence the effectiveness of the Double Filtering Method. The investigation then goes on to apply the method, investigating the effects of changing rotational speed on the broadband noise sources of counter-rotating open rotors, presenting the various categories of broadband noise sources and their occurrence on the beamforming maps and in the spectra. Four major categories are looked at as a function of rotational speed: two different blade angles (simulating take-off and approach conditions), and two different installations (uninstalled and installed with a pylon).

Keywords: beamforming, broadband noise sources, counter-rotating turbomachinery, signal processing

NOMENCLATURE

f	$\left[\frac{1}{min}\right]$	rotational speed
f_{NRNS}	[Hz]	frequency of the NRNS
L_{tot}	[s]	total loss
N	[-]	number of subsegments in a NRNS filtering segment
T_e	[s]	length of a Single filtered segment
T_{NRNS}	[s]	length of a subsegment

Subscripts and Superscripts

ideal	ideal value
max	maximal value
NRNS	non-rotational noise source

1. INTRODUCTION

Counter-Rotating Open Rotors (CROR) are made up of two unducted rotors. Their main advantage over single rotor turbomachinery is lower fuel consumption [1]. However, there are still many obstacles to overcome. Such as its high noise emission, which has been the subject of numerous investigations [2-10]. A sketch of a CROR test rig can be seen in Figure 1. The test rig consists of two rotors (two trapezoids) that are mounted on the hub. The flow is going from left to right, as the flow first interacts with a pylon before reaching the rotors. The pylon can optionally be removed, as marked by the dashed line. Downstream of the rotors, the rest of the test rig is sufficiently far away in order to not influence the flow around the rotors.

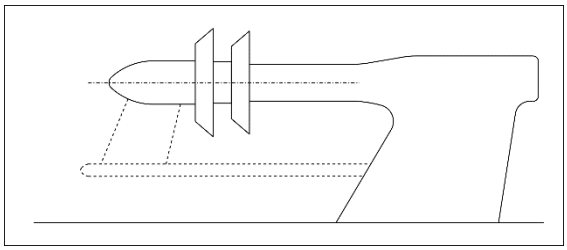

Figure 1. Sketch of a CROR test rig

CROR noise sources can be categorised in many ways [11-13]. This paper focuses on the broadband noise sources, which can be divided into four main groups [14]: Blade root noise sources, Trailing edge

noise sources, Leading edge noise sources, and Blade tip noise sources.

Another aspect of grouping is whether the noise source is located on the suction or pressure side. If it appears on a blade moving towards the observer, it is on the pressure side. If the blade moves away from the observer, the noise source is on the suction side. In our case, the forward blade row shows the pressure side above the shaft, and the suction side below it. The situation is exactly the opposite on the aft blade row, the suction side is visible above the shaft and the pressure side is visible below.

Blade root noise sources are located near the base of the blades on the aft rotor, both on the pressure and suction side. They are created by the interaction between the boundary layer on the shaft and the blade roots. An example of this is shown in Figure 2., marked with a square.

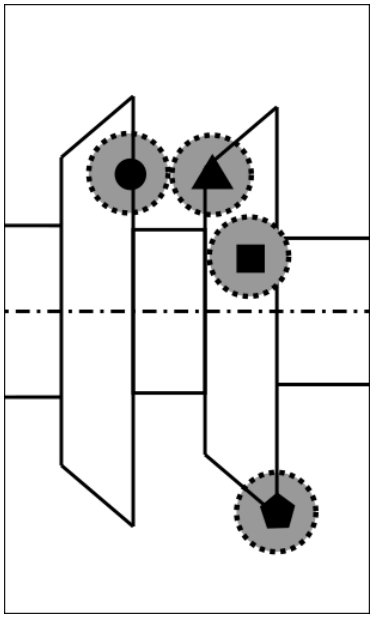

Figure 2. CROR noise sources

Trailing edge noise sources appear dominantly on the pressure side of the forward rotor. This noise source is more pronounced at higher frequencies. The typical region where these noise sources predominantly appear is shown in Figure 2., marked with a circle.

Leading edge noise sources are most significant on the aft blade row and can be seen near the leading edge on both the pressure and suction sides. The typical region where these noise sources predominantly appear is shown in Figure 2., marked with a triangle.

Blade tip noise sources can be seen on the pressure side of the aft rotor. The typical region where these noise sources predominantly appear is shown in Figure 2., marked with a pentagon.

The measurements discussed in this paper have been carried out in the NASA Glenn Research Center 9×15 ft Low-Speed Wind Tunnel, on a F31/A31 historic baseline CROR [15]. The forward rotor has 12 blades with a diameter of 0.652 m, while the aft rotor has 10 blades with a diameter of 0.63 m. The Mach number of the flow has been 0.2, and the angle of attack has been set to 0˚.

Table 1. Uninstalled, approach cases

Case number	Forward rotational speed $\left(\frac{1}{min}\right)$	Aft rotational speed $\left(\frac{1}{min}\right)$	Temp. [˚C]
U-A-5716	5716	5716	28.3
U-A-6463	6463	6463	28.5
U-A-7405	7405	7405	28.9
U-A-7653	7653	7653	29.1

Table 2. Uninstalled, take-off cases

Case number	Forward rotational speed $\left(\frac{1}{min}\right)$	Aft rotational speed $\left(\frac{1}{min}\right)$	Temp. [˚C]
U-T-4725	4725	4724	28.1
U-T-5390	5390	5390	28.4
U-T-5680	5680	5680	28.6
U-T-6211	6211	6212	28.7
U-T-6453	6453	6453	28.8
U-T-6590	6590	6590	28.9

Two different configurations have been investigated: Take-off ((T) blade angles: 40.1˚ for the forward, 40.8˚ for the aft rotor) and Approach ((A) blade angles: 33.5˚ for the forward, 35.7˚ for the aft rotor). Both configurations have been tested uninstalled (U) and installed with a pylon (P), which are support structures the engines (such as a CROR) are mounted on. Tables 1 to 4 contain the various investigated cases and the corresponding rotational speed values. Though the data presented in this paper is from an earlier investigation, this is the first investigation that presents a beamforming comparison of the broadband noise sources of all the test cases presented herein (Tables 1-4) as a function of rotational speed.

Table 3. Installed, approach cases

Case number	Forward rotational speed $\left(\frac{1}{min}\right)$	Aft rotational speed $\left(\frac{1}{min}\right)$	Temp. [˚C]
P-A-5754	5754	5754	32.3
P-A-6503	6503	6503	32.5
P-A-6967	6967	6966	32.7
P-A-7451	7451	7451	32.7
P-A-7700	7700	7700	32.9

Table 4. Installed, take-off cases

Case number	Forward rotational speed $\left(\frac{1}{min}\right)$	Aft rotational speed $\left(\frac{1}{min}\right)$	Temp. [°C]
P-T-4764	4764	4764	33.1
P-T-5430	5430	5430	33.1
P-T-5723	5723	5724	33.2
P-T-6258	6258	6258	33.3
P-T-6501	6501	6501	33.3

2. BEAMFORMING AND DOUBLE FILTERING

2.1 Phased array microphone system and beamforming

During the investigations, an OptiNAV Array48 phased array microphone system has been used, which contains 48 microphones [16]. Signals have been recorded at a sample rate of 96 kHz.

The method used to process the data measured with the phased array microphone system is called beamforming. The specific beamforming method chosen for this investigation has been Delay-and-sum beamforming, which has been found to provide a good signal-to-noise ratio with little loss of information. The data has been processed in the frequency domain [17]. This method is based on compensating the signals recorded by each microphone for every investigated point. This compensation is such that if a noise source exists in that investigated point, the compensated signals will be approximately the same for each microphone. Conversely, if there is no noise source at the investigated point, the compensated signals will be different. After compensating the signals, they are averaged for every investigated point. If a noise source exists in the investigated point, this value - called beamforming level - will be large. The output beamforming level is displayed on the beamforming maps (Figures 1 to 4).

2.2 Double filtering

Broadband noise sources typically have a smaller amplitude than tonal noise sources, which makes them difficult to study. This is especially difficult in the case of CROR, as the tonal noise components dominate many of the frequency bins, as seen in Figure 3, thus hiding the broadband noise components on the beamforming maps. In order to be able to investigate these noise sources, they must be separated from tonal noise sources.

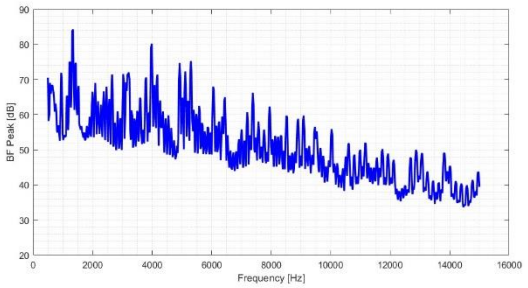

Figure 3. Typical CROR spectrum of the BF Peak value

The Double filtering method builds on a signal processing method developed by Sree and Stephens [18]. This signal processing method removes tonal components related to the rotational speed of a CROR, which are referred to herein as Rotational Noise Sources (RNS) [14]. The resulting signal is referred to herein as a Single filtered signal.

There are also other tonal noise components, which are not related to the rotational speed, called Non-Rotational Noise Sources (NRNS) [14]. In this investigation, a deer whistle, used to verify beamforming maps, is such a noise source. We can filter these noise sources out using a method developed by Tokaji et al. [19] called Double filtering. The resulting signal is called a Double filtered signal.

In carrying out Double filtering, first the signal must be split into segments. In filtering out the RNS components, these segments must be one revolution long [18]. Then, neighbouring segments must be subtracted from one another. This filters out the RNS components, as they repeat in each segment, due to their lengths being one revolution long. Finally, the resulting signal must be divided by $\sqrt{2}$, so that the resulting broadband signal has the same properties as the broadband components in the original signal [18-20].

The principle behind filtering out the NRNS component is similar to that of filtering out the RNS component. All Single filtered segments must be split into new, shorter segments, as seen in Figure 4.

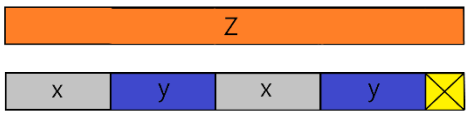

Figure 4. Splitting the signal into segments

While the choice of segment length is straightforward in the case of Single filtering, here

there are multiple options. The NRNS filtering segment length is based on the period time corresponding to the frequency of the NRNS. This is referred to herein as a subsegment [14]. Theoretically, this is the shortest applicable segment length in this case. However, the use of one subsegment long NRNS filtering segments is not recommended, because it is too short, which leads to a lot of information loss and inadequately filtered signals. It can also be stated that the length of the NRNS filtering segments must be shorter than half the length of a Single filtered segment. This is necessary in order to have at least two segments, which can be subtracted. The length of an NRNS filtering segment must be a multiple of the length of a subsegment.

3. PARAMETERS OF NRNS FILTERING, SEGMENT LENGTH

We have seen in the previous section that there are several options when it comes to choosing the NRNS filtering segment's length. First, the frequency of the NRNS (f_{NRNS}) must be determined. This varies slightly between the investigated cases, but it is approximately 3200 [Hz] in this study. Using f_{NRNS}, one can define the length of a subsegment (T_{NRNS}), as given in Eq. (1).

$$T_{NRNS} = \frac{1}{f_{NRNS}} \tag{1}$$

The length of a Single filtered segment (T_e) can be calculated using the rotational speed of the given case (f) as seen in Eq. (2).

$$T_e = \frac{60}{f} \tag{2}$$

Another important parameter of NRNS filtering is N, which is equal to the number of subsegments a NRNS filtering segment consists of. N must be an integer between 1 and N_{max}, which can be calculated as shown in Eq. (3), where [.] refers to the integer function.

$$N_{max} = \left[\frac{T_e}{2T_{NRNS}}\right] \tag{3}$$

The length of the NRNS filtered signal is shorter than the length of the original signal. This is the results of two major factors: segment fragments and a loss of an entire NRNS filtering segment in each Single filtered segment, due to the subtraction in the Double filtering method.

An example for a segment fragment can be seen in Figure 4., represented by the yellow rectangle. The Single filtered segment lengths (Z) are not multiples of the NRNS filtered segment lengths (x and y); hence such fragments are always present. These are lost during the filtering process.

The sum of these two types of losses is called the total loss (L_{tot}), which is related to the value of N. Our investigations have shown that the N corresponding to the maximum total loss ($N(L_{tot,max})$) is between 65% and 77% of the value of N_{max} for the investigated cases. It has been found that Double filtering yields the best results if the chosen N is lower than the one corresponding to the maximum of total loss for that given case.

It has also been stated in the previous chapter, that the use of too few subsegments (meaning N is small) leads to an inadequately filtered signal. During the investigation, every possible Double filtered signal (using all valid N values from 1 to N_{max}, as shown in Eq. 3) have been created for the CROR cases to study this phenomenon. In the investigated cases, $N = 7$ has been found to be the smallest N with which the Double filtered signal has been considered acceptable. Hence it has been chosen as the lower limit for the ideal value of N for these cases.

Combining these findings, the range containing the ideal value of N for the investigated cases is shown in Eq. (4).

$$7 \leq N < N(L_{tot,max}) \tag{4}$$

A trend showing that the ideal value for N is half of N_{max} has also been observed, which is true for most cases. If N_{max} is even, the formula seen in Eq. (5) has been used. If N_{max} is odd, the formula seen in Eq. (6) has been used.

$$N_{ideal} = \frac{(N_{max})}{2} \tag{5}$$

$$N_{ideal} = \frac{(N_{max} \mp 1)}{2} \tag{6}$$

The ideal and the maximum Double filtering segment length for each investigated case can be seen in Table 5. Unmarked cases are the ones for which the ideal value for N is half of N_{max}. Cases marked with yellow are the ones, for which N from Eq. (5) or (6) does not fit in the range defined in Eq. (4). Cases marked with red are the ones, which do not fit the trend at all. As this trend fits the investigated cases well, it can be used as a starting value for future studies and applications of the Double filtering method to other similar test cases.

Table 5. Ideal and maximum N values

Case number	N_{ideal}	N_{max}
U-A-5716	7	16
U-A-6463	7	14
U-A-7405	8	13
U-A-7653	8	12
P-T-4764	10	19
P-T-5430	8	17
P-T-5723	8	16
P-T-6258	7	15
P-T-6501	7	14
U-T-4725	10	19
U-T-5390	8	17
U-T-5680	8	16
U-T-6211	7	15
U-T-6453	7	14
U-T-6590	8	14
P-A-5754	8	16
P-A-6503	7	14
P-A-6967	7	13
P-A-7451	8	12
P-A-7700	8	12

4. INVESTIGATING AND COMPARING THE DOUBLE FILTERED SIGNALS AS A FUNCTION OF ROTATIONAL SPEED

Using the ideal Double filtered segment length shown in Table 5, Double filtered signals have been created for each investigated case. This has made it possible to examine the broadband noise sources with the help of beamforming maps and spectra, comparing the various test cases described in Tables 1-4.

The location of each noise source on the CROR examined during the investigation can be observed on the beamforming maps (Figures 9 to 17). These maps present the highest beamforming levels in a given frequency band and the 5 [dB] dynamic range below it, with the corresponding colour scale in the lower right corner of the figures. The upper left corner of the beamforming map shows the frequency band for that figure. The magnitude of the peak is located in the upper right corner. This value is called beamforming level

The Double filtered spectra for the uninstalled approach, the uninstalled take-off, the installed approach, and the installed take-off cases are shown in Figures 5-8, respectively. Comparing these spectra helps to identify differences between cases with varying rotational speeds, narrowing down the frequency bands of interest. In chapters 4.1 to 4.3, some of these frequency bands are investigated.

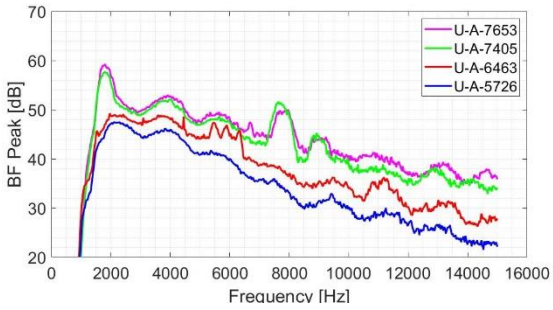

Figure 5. Uninstalled, approach broadband spectra

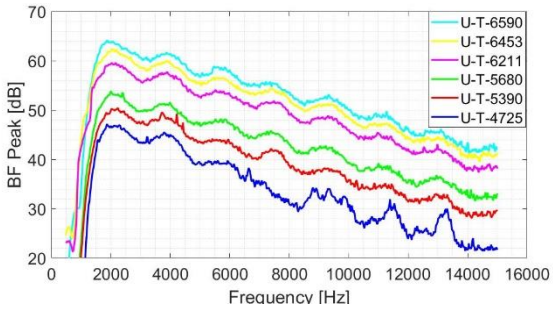

Figure 6. Uninstalled, take-off broadband spectra

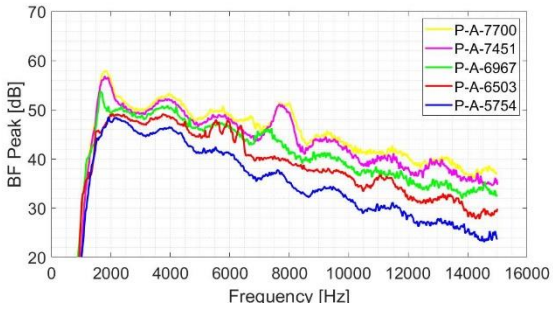

Figure 7. Installed, approach broadband spectra

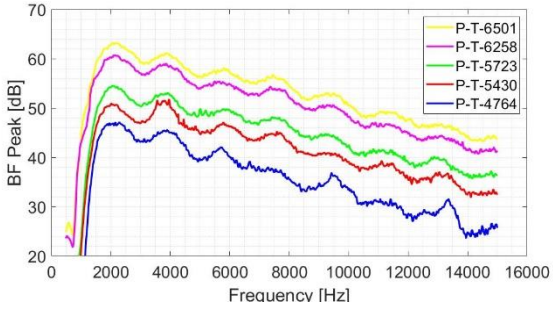

Figure 8. Installed, take-off broadband spectra

4.1 Comparison of approach cases with varied rotational speeds

For take-off mode cases, the shape of the Double filtered spectra have been found to be similar for the installed and uninstalled cases. It can also be seen

that cases with higher rotational speeds have larger beamforming peak levels across the entire frequency domain, as seen in Figures 5 and 7. On the other hand, approach mode cases differ greatly in some frequency bands.

First, a series of three peaks can be seen between 5500 Hz and 6500 Hz, for case numbers U-A-6463 and P-A-6503. These peaks are caused by Trailing edge noise sources, which are rarely found below 7000 Hz for the other cases in this study, and Blade tip noise sources while other cases have Blade root noise sources as their dominant noise source. This can be seen in Figure 9, for the uninstalled case.

Figure 9. Trailing edge and Blade tip noise source, case number U-A-6463

Second, a large increase in the magnitude of the beamforming levels can be observed between 7000 Hz and 8500 Hz, peaking around 7700 Hz for cases with higher rotational speeds (U-A-7405, U-A-7653 and P-A-7451, P-A-7700). The dominant noise sources have been Blade tip noise sources for every case in this frequency band in installed cases, but cases with lower rotational speeds have not produced an increase like this. In the uninstalled cases, case numbers U-A-5726 and U-A-6463 have Blade root noise sources and Trailing edge noise sources as their dominant ones, while the increase in magnitude for case numbers U-A-7405 and U-A-7653 has been caused by Blade tip noise sources, similarly to the installed cases. An example for this can be seen in Figure 10, for case number P-A-7700.

Figure 10. Blade tip noise source, case number U-A-7700

4.2 Trailing edge noise sources

Trailing edge noise sources appear most commonly on the forward rotor, on the pressure side. They dominate higher frequency bands. Investigations have shown that the pylon affects these noise sources.

Figure 11. Trailing edge noise source, uninstalled mode, case number U-T-6453

For uninstalled cases – both take-off and approach – Trailing edge noise sources have appeared above 7500 Hz and become more dominant at higher frequencies, as seen in Figure 11. However, for installed cases, Trailing edge noise sources have only started to appear above 10 kHz, for both take-off and approach settings. An example for a Trailing edge noise source can be seen in Figure 12.

Figure 12. Trailing edge noise source, installed mode, case number P-T-6501

4.3 The effect of a pylon and rotational speed on Blade tip noise sources

Blade tip noise sources appear on the pressure side of the aft rotor. They are greatly affected by both a presence of a pylon and the rotational speed.

Investigations have shown that Blade tip noise sources are more dominant in installed cases. In Figures 13 and 14, an installed and uninstalled case with similar rotating speeds can be seen. While in the installed case, the Blade tip noise source is clearly the dominant one, in the uninstalled case, a Blade root noise source can be seen.

Figure 13. Blade root noise source in the uninstalled case, case number U-T-4725

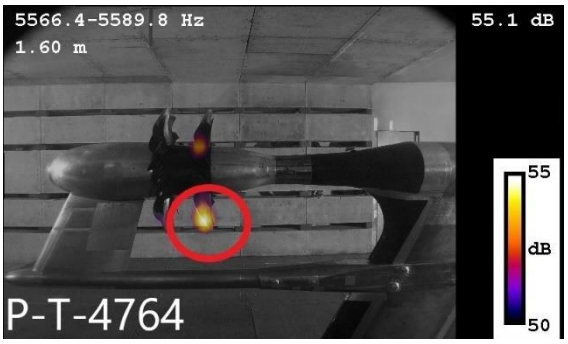

Figure 14. Blade tip noise source in the installed case, case number P-T-4764

The other main factor affecting Blade tip noise sources is the rotational speed, which can be best studied using the uninstalled cases. Investigations have shown that Blade tip noise sources become more dominant as the rotational speed increases. Figures 15 to 17 show uninstalled, take-off cases with various rotational speeds for the same frequency band. While for case number U-T-4725, the Blade root noise source is clearly the dominant source, in case number U-T-5680, we can see a Blade tip noise source appear. As we increase the rotational speed even further, the Blade tip noise sources become more and more dominant, as seen in Figure 17.

Figure 15. Investigating the effect of rotational speed on Blade tip noise, case number U-T-4725

Figure 16. Investigating the effect of rotational speed on Blade tip noise, case number U-T-5680

Figure 17. Investigating the effect of rotational speed on Blade tip noise, case number U-T-6590

5. CONCLUSIONS

In this study, the parameters of Double filtering have been investigated, focusing on ideal segment length. A subsegment and the value of N, which shows how many subsegments a NRNS filtering segment consist of, have been defined. For the investigated cases, a lower limit of 7 has been chosen for the value of N, because below this, Double filtering segments are too short, leading to inadequately filtered signals. An upper limit has been chosen as well, with the help of total loss, which shows how much shorter the Double filtered signal is, as compared to the original signal. The upper limit has a value for N which corresponds to the maximum total loss for each given case. Another trend worth mentioning is that the ideal value for N has half the value of the maximum N, which has been true for 18 of the 20 investigated cases.

Using the ideal segment length, Double filtered signals have been created for every case. The spectra of the take-off cases have been similarly shaped, cases with higher rotational speeds have larger beamforming peak levels across the entire frequency domain. On the other hand, the spectra of approach cases have shown two main differences between cases with different rotational speeds. These have been consistent for both installed and uninstalled cases.

When comparing Trailing edge noise sources in the take-off and approach cases, we have reached the

conclusion that in the installed case, these type of noise sources appear from 10 kHz. In the uninstalled cases, they can be seen from 7500 Hz

Blade tip noise sources have been affected by two main factors: rotational speed and the presence of the pylon. Investigations have shown that Blade tip noise is more dominant in installed cases. Higher rotational speeds result in more dominant Blade tip noise sources as well, best demonstrated by the uninstalled, take-off cases.

ACKNOWLEDGEMENTS

The research reported in this paper and carried out at BME has been supported by the Hungarian NRDI Centre under contract No. K 129023, by the NRDI Fund (TKP2020 NC, Grant No. BME-NCS) based on the charter of bolster issued by the NRDI Office under the auspices of the Ministry for Innovation and Technology, and is part of project no. BME-NVA-02, implemented with the support provided by the Ministry of Innovation and Technology of Hungary from the NRDI Fund, financed under the TKP2021 funding scheme.

REFERENCES

[1] Bowles, M. D., 2010, ""Apollo" of Aeroacoustics: NASA's Aircraft Energy Efficiency Program 1973-1987," NASA Headquarters, Washington, D.C., USA, 113-140

[2] Woodward, R. P., 1987, "Noise of a Model High Speed Counterrotation Propeller at Simulated Takeoff/Approach Conditions (F7/A7)," NASA TM-100206, https://doi.org/10.2514/6.1987-2657

[3] Blandeau, V. P., Joseph, P. F., 2010, "Broadband Noise Due to Rotor-Wake/Rotor Interaction in Contra-Rotating Open Rotors", AIAA Journal, Vol. 48, No. 11, https://doi.org/10.2514/1.J050566

[4] Smith, D. A., A. Filippone, and N. Bojdo., 2020, "Noise reduction of a Counter Rotating Open Rotor through a locked blade row." Aerospace Science and Technology, Vol. 98 No. 105637., https://doi.org/10.1016/j.ast.2019.105637

[5] Yu, L., Wu, H., Antoni, J., & Jiang, W., 2019, "Extraction and imaging of aerodynamically generated sound field of rotor blades in the wind tunnel test", Mechanical Systems and Signal Processing, Vol. 116, pp. 1017-1028., https://doi.org/10.1016/j.ymssp.2018.07.042

[6] Fenyvesi, B., Kriegseis, J. and Horváth, Cs., 2019, "Application of a Combined Method for the Investigation of Turbomachinery Noise Sources: Beamforming and Proper Orthogonal Decomposition", 25th AIAA/CEAS Aeroacoustics Conference, AIAA 2019-2637, Delft, The Netherlands, https://arc.aiaa.org/doi/10.2514/6.2019-2637

[7] Funke, S., Kim, L. and Siller, H. A., 2011, "Microphone-Array Measurements of a Model Scale Contra-Rotating Open Rotor in a Reverberant Open Wind-Tunnel", 17th AIAA/CEAS Aeroacoustics Conference, Portland, OR, USA, AIAA 2011-2766, https://doi.org/10.2514/6.2011-2766

[8] Van Zante, D. E., Gazzaniga, J. A., Elliott, D. M., et al., 2011, "An Open Rotor Test Case: F31/A31 Historical Baseline Blade Set", 20th International Symposium on Airbreathing Engines, Gothenburg, Sweden, ISABE 2011-1310,

[9] Ricouard, J., Julliard, E., Omais, M., Regnier, V., Parry, A., Baralon, S., 2010, "Installation effects on contra-rotating open rotor noise", 16th AIAA/CEAS aeroacoustics conference, pp. 3795., https://doi.org/10.2514/6.2010-3795

[10] Elliott, D., 2011, "Initial investigation of the acoustics of a counter rotating open rotor model with historical baseline blades in a low-speed wind tunnel", 17th AIAA/CEAS Aeroacoustics Conference (32nd AIAA Aeroacoustics Conference), pp. 2760., https://doi.org/10.2514/6.2011-2760

[11] Fenyvesi, B., Tokaji, K., Horváth, Cs., 2019, "Investigation pf a Pylons Effect on the Character of Counter-Rotating Open Rotor Noise Using Beamforming Technology", Acta Acustica United With Acustica, Vol. 105, https://doi.org/10.3813/AAA.919287

[12] Horváth, Cs., Envia, E. and Podboy, G. G., 2014, "Limitations of Phased Array Beamforming in Open Rotor Noise Source Imaging", AIAA Journal, Vol. 52, No. 8, https://doi.org/10.2514/1.J052952

[13] Horváth, Cs., 2015, "Beamforming Investigation of Dominant Counter-Rotating Open Rotor Tonal and Broadband Noise Sources", AIAA Journal, Vol. 53, No. 6, https://doi.org/10.2514/1.J053465

[14] Tokaji, K., Horváth, Cs., 2021, "Effect of a pylon on the broadband noise sources of counter-rotating turbomachinery", International Journal of Aeroacoustics, Vol: 20 No. 8, pp. 979-1002 https://doi.org/10.1177/1475472X211055178

[15] Van Zante, D. E., 2013, "The NASA Environmentally Responsible Aviation Project", 51st AIAA Aerospace Sciences Meeting, https://doi.org/10.2514/6.2013-415

[16] Optinav Inc., Array 48, 2017, https://www.optinav.info/Array48

[17] Mueller, T. J., 2002, “Aeroacoustic Measurements.” Springer Verlag, Berlin, Germany, http://dx.doi.org/10.1017/S0022112003238398

[18] Sree D. and Stephens D. B., 2016, “Improved separation of tone and broadband noise components from open rotor acoustic data.” Aerospace, Vol. 3, No. 3, https://doi.org/10.3390/aerospace3030029

[19] Tokaji, K., Soós Bálint, Horváth, Cs., 2020, “Beamforming method for extracting the broadband noise sources of counter-rotating open rotors”, AIAA Journal, Vol. 58, No 7, https://doi.org/10.2514/1.J058934

[20] Sree, D., “A novel signal processing technique for separating tonal and broadband noise components from counter-rotating open-rotor acoustic data”, International Journal of Aeroacoustics, Vol. 12, No. 1-2, 2013, pp. 169-188., https://doi.org/10.1260/1475-472X.12.1-2.169